# Relativistic density-dependent Hartree-Fock approach for finite nuclei

Hua-lin Shi and Bao-qiu Chen
*China Institute of Atomic Energy, Beijing 102413, People's Republic of China*

Zhong-yu Ma
*China Center of Advanced Science and Technology (World Laboratory), P.O. Box 8730, Beijing 100080, People's Republic of China*
*and China Institute of Atomic Energy, Beijing 102413, People's Republic of China*
(Received 12 December 1994)

The nucleon self-energy obtained from the Dirac Brueckner-Hartree-Fock calculation is parametrized by introducing density-dependent coupling constants of isoscalar mesons in the relativistic Hartree-Fock (RHF) approach. The RHF calculations with density-dependent coupling constants not only reproduce the nuclear matter saturation properties, but also provide a good starting point to study finite nuclei properties. The relativistic density-dependent Hartree-Fock (RDHF) approach contains the features of the relativistic $G$ matrix and in the meantime simplifies the calculation. The ground state properties of spherical nuclei calculated in the RDHF are in good agreement with the experimental data. The contribution of isovector mesons $\pi$ and $\rho$, especially the contribution of the tensor coupling of $\rho$ mesons, are discussed in this paper.

PACS number(s): 21.60.Jz, 21.10.Dr, 21.65.+f, 24.10.Jv

## I. INTRODUCTION

In recent years, many investigations have been devoted to a relativistic description of nuclear properties. The relativistic mean field (RMF) theory with nonlinear self-interactions has turned out to be a very powerful tool in the description of the ground state properties of both spherical and deformed nuclei over the entire range of the periodic table [1,2]. Recently, it has also been demonstrated that the RMF is able to describe the properties of nuclei far from the stability line [3,4]. The relativistic Hartree-Fock (RHF) approach is an extension of the RMF. The contribution of the exchange terms in the RHF has been investigated, and the importance of the isovector mesons in the description of the ground state properties of nuclei has been emphasized [5–7]. In spite of the success of the RMF and RHF, however, too large a compressibility of nuclear matter is produced in these approaches. It might indicate an incorrect density behavior of the effective interaction described in the RMF and RHF approaches. It is known that the calculations in the RMF or RHF yield correct binding energies but too small a charge radius or vice versa. Such calculations reveal a new "Coester" band in the dependence of $1/r_{ch}$ on $E_B$, which is similar to that observed in the nonrelativistic Brueckner-Hartree-Fock (BHF) approach [8]. The deficiency of the RMF and RHF approaches might be attributed to the fact that the nucleon-nucleon short range correlations have not been taken into account in these approaches.

In taking account of the nucleon-nucleon short range correlation one starts from a bare nucleon-nucleon interaction of the one-boson-exchange potential, and solves the relativistic Brueckner-Goldstone equation in the nuclear medium [9–12]. The Dirac-Brueckner-Hartree-Fock (DBHF) approach quantitatively reproduces the empirical saturation properties of nuclear matter, such as the binding energy per nucleon and saturation density as well as the compressibility [11,13]. This implies that the nucleon self-energy in the nuclear medium obtained in the DBHF has a proper behavior in the density dependence. However, the DBHF due to its complexity is mainly restricted to nuclear matter and only very few finite nuclei calculations have been performed so far [14]. To extend the DBHF to finite nuclei, relativistic effective interactions are adopted to incorporate the DBHF results in the RMF or RHF, which is desired to remedy the deficiencies of the RMF or the RHF without losing the features of the relativistic $G$ matrix and at the same time to retain the simplicity of the calculations.

Recently, there is a growing effort to develop the relativistic effective interactions. Attempts have also been made to improve both binding energy and rms radii of finite nuclei simultaneously in the RMF or RHF with various effective interactions. These approaches introduce a density dependence into the hadronic Lagrangian by allowing the meson-nucleon coupling constants to be functionals of the baryon density. Gmuca [15] has parametrized the results of the DBHF in nuclear matter in terms of the RMF with scalar and vector nonlinear self-interactions. Though the coupling constants obtained in such a way are density independent, these mesonic self-interactions implicitly represent the density dependence. Brockmann and Toki [16] developed a relativistic density-dependent Hartree (RDH) approach for finite nuclei. The coupling constants of the isoscalar $\sigma$ and $\omega$ mesons in the RMF are adjusted at each density by reproducing the nucleon self-energies resulting from the DBHF instead of fitting to the empirical nuclear matter saturation properties. The binding energies and rms radii of $^{16}$O and $^{40}$Ca calculated with the density-dependent in-

 

teraction are in good agreement with experiments. However, Fritz, Müther, and Machleidt [17] pointed out that the Fock terms are not negligible and relativistic density-dependent Hartree-Fock (RDHF) calculations have been investigated. At very low densities the DBHF results are unknown and an extrapolation procedure has to be adopted for the calculations of finite nuclei. Due to the fact that there is no direct restriction on the coupling constants at very low density, in Ref. [18] the scalar and vector potentials of the DBHF results were extrapolated at low densities first by respecting their properties in nuclear matter. Then, the extrapolation of the coupling constants in the RDH or RDHF approaches is restricted by reproducing those scalar and vector potentials at the low densities. Therefore the coupling constants at the low densities in different approaches, the RDH or RDHF, are obtained on an equal level.

As mentioned above, the contributions of isovector mesons are neglected in Refs. [16,17]. It is known that a realistic description of the nucleon-nucleon interaction in terms of meson exchange must include $\pi$ and $\rho$. Therefore it is necessary to develop a relativistic theory for finite nuclei in the RHF including the isovector $\pi$ and $\rho$ mesons. Fritz and Müther [19] discussed the contribution of the pion to the bulk properties of finite nuclei in the RDHF approach. They found that the inclusion of the $\pi$-exchange terms in the RDHF slightly improves the agreement with the experiments. Boersma and Malfliet [20] achieved a density-dependent parametrization of the Dirac-Brueckner $G$ matrix in nuclear matter, which was called an effective DBHF. They used the effective DBHF to systematically analyze a series of spherical nuclei, and the results are in good agreement with the experiments. In our previous Brief Report [21], the effects of the isovector $\rho$ meson with a vector coupling in the RDHF on the bulk properties for finite nuclei were discussed. It was found that the exchange terms in the $\sigma$-$\omega$ model reduce the charge radii, but have less influence on the binding energies. A large repulsion of the $\pi$ contribution at the interior of nuclei is observed. As a result the energy levels of single particles become shallow in the presence of a $\pi$ meson. Therefore the total binding energy is reduced and the charge radius is expanded. This effect is partly canceled when the $\rho$ meson is included. But the contribution of tensor coupling of the $\rho$ meson has not been taken into account in these works. In this paper, the contribution of the isovector-vector $\rho$ meson, especially the effect of the tensor coupling of the $\rho$ meson on the ground state properties, is investigated in the RDHF approach. The RDHF results are compared with those obtained from other models and the experiments. A systematic study of finite nuclei in terms of the RDHF approach is carried out.

The arrangement of this paper is as follows. The general formalism in this work is presented in Sec. II. The numerical results and main conclusions are included in Secs. III and IV.

## II. THE FORMALISM

As in the one-boson-exchange (OBE) description of the nucleon-nucleon interaction [22], our starting point is an effective Lagrangian density which couples a nucleon ($\psi$) to two isoscalar mesons ($\sigma$, $\omega$) and two isovector ones ($\pi$, $\rho$) with the following quantum number ($J^\pi, T$): $\sigma(0^+,0)$, $\omega(1^-,0)$, $\pi(0^-,1)$, and $\rho(1^-,1)$. The electromagnetic field ($A^\mu$) is also included.

The effective Lagrangian density can be written as the sum of free and interaction parts:

$$\mathcal{L} = \mathcal{L}_0 + \mathcal{L}_I. \tag{1}$$

The free Lagrangian density is given by

$$\begin{aligned}\mathcal{L}_0 = {}& \bar{\psi}(i\gamma_\mu\partial^\mu - M)\psi + \frac{1}{2}(\partial_\mu\sigma\partial^\mu\sigma - m_\sigma^2\sigma^2) \\ & + \frac{1}{2}m_\omega^2\omega_\mu\omega^\mu \\ & - \frac{1}{4}F_{\mu\nu}F^{\mu\nu} + \frac{1}{2}m_\rho^2\rho_\mu\cdot\rho^\mu - \frac{1}{4}\mathbf{G}_{\mu\nu}\cdot\mathbf{G}^{\mu\nu} \\ & + \frac{1}{2}(\partial_\mu\pi\cdot\partial^\mu\pi - m_\pi^2\pi^2) - \frac{1}{4}H_{\mu\nu}H^{\mu\nu},\end{aligned} \tag{2}$$

with

$$\begin{aligned}F_{\mu\nu} &= \partial_\nu\omega_\mu - \partial_\mu\omega_\nu, \\ \mathbf{G}_{\mu\nu} &= \partial_\nu\rho_\mu - \partial_\mu\rho_\nu, \\ H_{\mu\nu} &= \partial_\nu A_\mu - \partial_\mu A_\nu,\end{aligned}$$

where the meson fields are denoted by $\sigma$, $\omega_\mu$, $\rho_\mu$, and $\pi$, and $m_\sigma$, $m_\omega$, $m_\rho$, and $m_\pi$ are their masses, respectively. The nucleon field is denoted by $\psi$, which has a rest mass $M$. $A_\mu$ is the electromagnetic field. The interaction Lagrangian density is given by

$$\begin{aligned}\mathcal{L}_I = {}& g_\sigma\bar{\psi}\sigma\psi - g_\omega\bar{\psi}\gamma_\mu\omega^\mu\psi - g_\rho\bar{\psi}\gamma_\mu\rho^\mu\cdot\tau\psi \\ & + \frac{f_\rho}{2M}\psi\sigma_{\mu\nu}\partial^\mu\rho^\nu\cdot\tau\psi - e\bar{\psi}\gamma_\mu\frac{1}{2}(1+\tau_3)A^\mu\psi \\ & - \frac{f_\pi}{m_\pi}\psi\gamma_5\gamma_\mu\partial^\mu\pi\cdot\tau\psi,\end{aligned} \tag{3}$$

where $\tau$ and $\tau_3$ are the isospin Pauli matrices. The effective strengths of couplings between the mesons and nucleons are denoted by the coupling constants $g_i$ or $f_i$ ($i = \sigma, \omega, \rho, \pi$), respectively. Note that the pseudovector (PV) coupling for $\pi NN$ interaction is used. It is known that the baryon self-energies become extremely large (about 40 times larger than their PV counterpart) at normal nuclear density if a pseudoscalar coupling is used, which has a drastic effect on the single-particle spectrum [23]. The present of tensor couplings makes the model Lagrangian density no longer renormalizable and all physical observables should be calculated at the tree level.

### A. Equations of motion

The equations of motion for meson fields are easily obtained from the Euler-Lagrange equation

$$\frac{\partial\mathcal{L}}{\partial\phi} - \partial_\mu\frac{\partial\mathcal{L}}{\partial(\partial^\mu\phi)} = 0, \tag{4}$$

with a meson field $\phi$. For instance, the $\sigma$ and $\omega$ fields are the solutions of

$$(\Box + m_\sigma^2)\sigma = g_\sigma \bar{\psi}\psi, \tag{5}$$

$$(\Box + m_\omega^2)\omega_\nu = g_\omega \bar{\psi}\gamma_\nu\psi, \tag{6}$$

with the baryon current conservation $\partial^\mu(\bar{\psi}\gamma_\mu\psi) = 0$. Solving these equations for meson fields, one then obtains

$$\sigma(x) = g_\sigma \int d^4y D_\sigma(x-y)\bar{\psi}(y)\psi(y), \tag{7}$$

$$\omega^\mu(x) = g_\omega \int d^4y D_\omega^{\mu\nu}(x-y)\bar{\psi}(y)\gamma_\nu\psi(y), \tag{8}$$

where $D_\sigma(x-y)$ and $D_\omega^{\mu\nu}(x-y)$ are the $\sigma$ and $\omega$ meson propagators, respectively. Similar expressions can be deduced for isovector mesons.

Following standard techniques [24], at the Hartree-Fock level, the expectation value of the Hamiltonian in the ground state can be written as

$$\begin{aligned}\langle\Phi_0|H|\Phi_0\rangle = \sum_\alpha \Bigg\{ &\int U_\alpha^\dagger(x)[-i\alpha\cdot\nabla + \gamma_0 m]U_\alpha(x)dx \\ &+ \int U_\alpha^\dagger(x)\gamma_0\Sigma_H(x)U_\alpha(x)dx \\ &- \int U_\alpha^\dagger(x)\gamma_0 \int \Sigma_F(x,y)U_\alpha(y)dydx \Bigg\},\end{aligned} \tag{9}$$

where $U_\alpha(x)$ is the nucleon wave function and satisfies the orthogonality relation

$$\int dy U_\alpha^\dagger(y)U_\beta(y) = \delta_{\alpha\beta}.$$

Only positive-energy states have been taken into account in the preceding derivation.

### B. Nuclear matter

Because of the translational and rotational invariance in the rest frame of infinite nuclear matter and the assumed invariance under parity and time reversal, the nucleon self-energy produced by the meson exchanges in nuclear matter can, in general, be written as

$$\Sigma(k_\nu) = \Sigma_s(k_\nu) - \gamma_0\Sigma_0(k_\nu) + \gamma\cdot\mathbf{k}\Sigma_v(k_\nu), \tag{10}$$

where $\Sigma_s$, $\Sigma_0$, and $\Sigma_v$ denote the scalar and time and space components of vector potentials, respectively. In general, they are functions of the four-momentum $k_\nu$ of a nucleon and the Fermi momentum $k_F$. Based on the Feynman diagram rules one could derive the nucleon self-energy in nuclear matter. In the RHF approach, the isoscalar mesons in our Lagrangian density give rise to the following contributions to the self-energy [23,25]:

$$\begin{aligned}\Sigma_s(k_\nu) = &-\left(\frac{g_\sigma}{m_\sigma}\right)^2\rho_s + \frac{1}{16\pi^2 k}\int_0^{k_F} dqq\hat{M}(q_0) \\ &\times[g_\sigma^2\Theta_\sigma(k,q) - 4g_\omega^2\Theta_\omega(k,q)],\end{aligned} \tag{11}$$

$$\begin{aligned}\Sigma_0(k_\nu) = &-\left(\frac{g_\omega}{m_\omega}\right)^2\rho_B - \frac{1}{16\pi^2 k}\int_0^{k_F} dqq[g_\sigma^2\Theta_\sigma(k,q) \\ &+2g_\omega^2\Theta_\omega(k,q)],\end{aligned} \tag{12}$$

$$\begin{aligned}\Sigma_v(k_\nu) = &-\frac{1}{(8\pi^2k^2)}\int_0^{k_F} dqq\hat{Q}(q_\nu)[g_\sigma^2\Phi_\sigma(k,q) \\ &+2g_\omega^2\Phi_\omega(k,q)],\end{aligned} \tag{13}$$

where

$$\hat{M}(q_\nu) = \frac{M^*(q_\nu)}{q_0^*(q_\nu)}, \qquad \hat{Q}(q_\nu) = \frac{q^*(q_\nu)}{q_0^*(q_\nu)},$$

$$\Theta_i(k,q) = \ln\left|\frac{(k+q)^2+m_i^2}{(k-q)^2+m_i^2}\right|,$$

$$\Phi_i(k,q) = \frac{k^2+q^2+m_i^2}{4kq}\Theta_i(k,q) - 1, \quad i = \sigma,\omega,\rho,\pi\ ,$$

$$\mathbf{k}^* = \mathbf{k}[1+\Sigma_v(k_\nu)], \quad k^* = |\mathbf{k}^*|,$$

$$M^* = M + \Sigma_s(k_\nu),$$

$$k_0^* = k_0 + \Sigma_0(k_\nu) = (k^{*2} + M^{*2})^{1/2}.$$

The scalar and vector densities are

$$\rho_s = \frac{2}{\pi^2}\int_0^{k_F} q^2\hat{M}(q)dq,$$

$$\rho_B = \frac{2}{3\pi^2}k_F^3. \tag{14}$$

The contributions of the isovector $\pi$ and $\rho$ mesons to the self-energy are given in Appendix A. The first terms of $\Sigma_s$ and $\Sigma_0$ in Eqs. (11) and (12) are the Hartree terms, which are momentum independent. The rest terms are the Fock terms, which are almost $1/k$ dependent. The coupled nonlinear integral equations of the self-energies, Eqs. (11)–(13) have to be solved self-consistently .

Requiring that the nucleon self-energies produced in the RMF or RHF are the same as those obtained in the DBHF at each baryon density, one can adjust the coupling constants $g_\sigma$ and $g_\omega$ as functions of the baryon density. The detailed procedure will be discussed in Sec. III A.

### C. Finite nuclei

In the case of spherical, closed-subshell nuclei, a single-particle baryon state with energy $E_\alpha$ is specified by the set of quantum numbers

$$\alpha = (q_\alpha, n_\alpha, l_\alpha, j_\alpha, m_\alpha) \equiv (a, m_\alpha),$$

where $q_\alpha = +1(-1)$ for a proton (neutron) state. The nucleon wave function can be written as

$$U_\alpha(x) = \frac{1}{r}\begin{pmatrix} iG_a(r) \\ F_a(r)\sigma\cdot\hat{\mathbf{r}}\end{pmatrix}\mathcal{Y}_\alpha(\hat{r})\chi_{1/2}(q_\alpha), \tag{15}$$

where $\chi_{1/2}(q_\alpha)$ is an isospinor, and the angular and spin

parts of the nucleon spinor can be written as

$$\mathcal{Y}_\alpha(\hat{r}) = \sum_{\mu_\alpha, s_\alpha} \left\langle l_\alpha \frac{1}{2} \mu_\alpha s_\alpha \middle| j_\alpha m_\alpha \right\rangle Y_{l_\alpha}^{\mu_\alpha}(\hat{\mathbf{r}}) \chi_{1/2}(s_\alpha).$$

The spinors $U_\alpha(r)$ are normalized according to

$$\int d^3\mathbf{r} U_\alpha^\dagger(x) U_\alpha(x) = \int_0^\infty [G_a^2(r) + F_a^2(r)] dr = 1.$$

The Hartree-Fock solution is obtained by requiring that the total binding energy

$$E = \langle \phi_0 | H | \phi_0 \rangle - AM$$

is stationary with respect to variations of the spinors $U_\alpha$ (i.e., of $G_\alpha$ and $F_\alpha$) such that the normalization relation is preserved,

$$\delta \left[ E - \sum_{\alpha(\text{occ})} E_\alpha \int U_\alpha^\dagger(r) U_\alpha(r) d^3r \right] = 0. \tag{16}$$

After a lengthy derivation, one can obtain the Hartree-Fock equations for the self-consistent wave functions $(G_\alpha, F_\alpha)$ and energies $E_\alpha$. The radial Dirac equations take the following form:

$$\frac{d}{dr} \begin{pmatrix} G_a(r) \\ F_a(r) \end{pmatrix} = \begin{pmatrix} -\frac{\kappa_\alpha}{r} - \Sigma_{T,a}^D(r) & M + E_\alpha + \Sigma_{S,a}^D(r) - \Sigma_{0,a}^D \\ M - E_\alpha + \Sigma_{S,a}^D(r) + \Sigma_{0,a}^D & \frac{\kappa_\alpha}{r} + \Sigma_{T,a}^D(r) \end{pmatrix} \begin{pmatrix} G_a(r) \\ F_a(r) \end{pmatrix} + \begin{pmatrix} -X_\alpha(r) \\ Y_\alpha(r) \end{pmatrix}, \tag{17}$$

where $\Sigma_{S,a}^D$, $\Sigma_{0,a}^D$, and $\Sigma_{T,a}^D$ are the contributions of the direct terms to the self-energy and can be expressed as follows:

$$\Sigma_{T,a}^D(r) = [\Sigma_\rho^T(r) + \Sigma_\rho^{VT(1)}(r)] q_\alpha, \tag{18}$$

$$\Sigma_{S,a}^D(r) = \Sigma_\sigma(r), \tag{19}$$

$$\Sigma_{0,a}^D(r) = \Sigma_\omega(r) + [\Sigma_\rho^V(r) + \Sigma_\rho^{VT(2)}(r)] q_\alpha + \frac{1}{2}(1 + q_\alpha)\Sigma_c(r), \tag{20}$$

and $X_\alpha$ and $Y_\alpha$ come from the exchange (Fock) contribution. The quantity $\kappa_\alpha$ is $(2j_\alpha + 1)(l_\alpha - j_\alpha)$.

In this work we consider nuclei with a closed proton and neutron shell only; therefore the isovector pseudoscalar meson yields no contribution in the Hartree approximation. The Hartree contributions, which come from $\sigma$, $\omega$, and $\rho$ mesons and the Coulomb force, are given as

$$\Sigma_\sigma(r) = -g_\sigma[\rho_B(r)] m_\sigma \int_0^\infty g_\sigma[\rho_B(r')] \rho_S(r') \times \tilde{I}_0(m_\sigma r_<) \tilde{K}_0(m_\sigma r_>) r'^2 dr', \tag{21}$$

$$\Sigma_\omega(r) = g_\omega[\rho_B(r)] m_\omega \int_0^\infty g_\omega[\rho_B(r')] \rho_B(r') \times \tilde{I}_0(m_\omega r_<) \tilde{K}_0(m_\omega r_>) r'^2 dr', \tag{22}$$

$$\Sigma_\rho^V(r) = g_\rho^2 m_\rho \int_0^\infty [\rho_{B,p}(r') - \rho_{B,n}(r')] \times \tilde{I}_0(m_\rho r_<) \tilde{K}_0(m_\rho r_>) r'^2 dr', \tag{23}$$

$$\Sigma_\rho^{VT(1)}(r) = -\frac{f_\rho}{2M g_\rho} \frac{d}{dr} \Sigma_\rho^V(r), \tag{24}$$

$$\Sigma_\rho^{VT(2)}(r) = -\frac{g_\rho f_\rho}{2M} m_\rho \int_0^\infty [\rho_{T,p}(r') - \rho_{T,n}(r')] \times \left[ \frac{d}{dr'} \tilde{I}_0(m_\rho r_<) \tilde{K}_0(m_\rho r_>) \right] r'^2 dr', \tag{25}$$

$$\Sigma_\rho^T(r) = -\left( \frac{f_\rho}{2M} \right)^2 \left\{ m_\rho^3 \int_0^\infty [\rho_{T,p}(r') - \rho_{T,n}(r')] \times \tilde{I}_1(m_\rho r_<) \tilde{K}_1(m_\rho r_>) r'^2 dr' - [\rho_{T,p}(r) - \rho_{T,n}(r)] \right\}, \tag{26}$$

$$\Sigma_c(r) = e^2 \int_0^\infty \frac{\rho_{B,p}(r')}{r_>} r'^2 dr' \tag{27}$$

with the definitions

$$\rho_{S,n \text{ or } p} = \frac{1}{4\pi r^2} \sum_{b(n \text{ or } p)} \hat{j}_b^2 [G_b^2(r) - F_b^2(r)],$$

$$\rho_{B,n \text{ or } p} = \frac{1}{4\pi r^2} \sum_{b(n \text{ or } p)} \hat{j}_b^2 [G_b^2(r) + F_b^2(r)],$$

$$\rho_{T,n \text{ or } p} = \frac{1}{4\pi r^2} \sum_{b(n \text{ or } p)} \hat{j}_b^2 [2 G_b(r) F_b(r)],$$

and $r_<$ ($r_>$) is the smaller (larger) of $r'$ and $r$.

The functions $\tilde{I}_L(x)$ and $\tilde{K}_L(x)$, which arise from the multiple expansion of the meson propagator in the coordinate space, are defined by using the modified spherical Bessel functions of the first and third kind $I$ and $K$:

$$\tilde{I}_L(x) = \frac{I_{L+\frac{1}{2}}(x)}{\sqrt{x}}, \qquad \tilde{K}_L(x) = \frac{K_{L+\frac{1}{2}}(x)}{\sqrt{x}}.$$

The explicit expressions of exchange contributions $X_\alpha$ and $Y_\alpha$ are given in Appendix B.

## III. RESULTS AND DISCUSSION

### A. Parametrization of DBHF

The self-energy obtained in the RHF shows a weak dependence on the momentum of the nucleon and a strong dependence on the density of the system. It is known that the resulting saturation curve is too strongly density dependent, which might be due to the fact that the short range correlation has not been considered in the RMF or RHF approaches. Attempts have been made to incorporate the effects of the short range correlation described in the DBHF approach by introducing density- and momentum-dependent effective coupling constants of isoscalar mesons in the RHF approach [17,20,21,26].

In order to make comparison with the DBHF results, the scalar and vector potentials in the RHF approach can be obtained by

$$U_s(k,k_F) = \frac{\Sigma_s - M\Sigma_v}{1+\Sigma_v}, \quad U_0(k,k_F) = \frac{-\Sigma_0 + E_k\Sigma_v}{1+\Sigma_v}, \tag{28}$$

where $E_k = \sqrt{k^{*2}+M^{*2}} - \Sigma_0$. The momentum dependence of the potentials is usually relatively weak and neglected in the description of ground state properties of finite nuclei. Therefore the momentum average within the Fermi sea is performed,

$$U_{s(0)}(k_F) = \frac{\int_0^{k_F} k^2 U_{s(0)}(k,k_F)\, dk}{\int_0^{k_F} k^2\, dk}. \tag{29}$$

At very low density of nuclear matter the DBHF results are not reliable and remain unknown. Therefore the extrapolation of the coupling constants outside the density points in the DBHF has to be done when they are applied to the calculation of finite nuclei. In order to remove the sensitivity, the extrapolation of scalar and vector potentials $U_s$ and $U_0$ of the DBHF results at low densities is done by setting $U_s = 0$, $U_0 = 0$ at $\rho_B = 0$. It is known that the scalar and vector potentials in the RMF or RHF are almost linearly dependent on the density. Due to the short range $NN$ correlation the scalar and vector potentials approach zero smoothly as the density goes to zero. A polynomial fit of the scalar and vector potentials with respect to the density is performed. The extrapolation and interpolation of $U_s$ and $U_0$ are shown in Fig. 1, where the circles are the DBHF results in nuclear matter using the Bonn $A$ potential [13]. The density dependence of the coupling constants is then adjusted in the cases of the RMF or RHF with or without isovector mesons to reproduce the nucleon self-energies at each density resulting from the DBHF. The masses of the nucleon and $\sigma$ and $\omega$

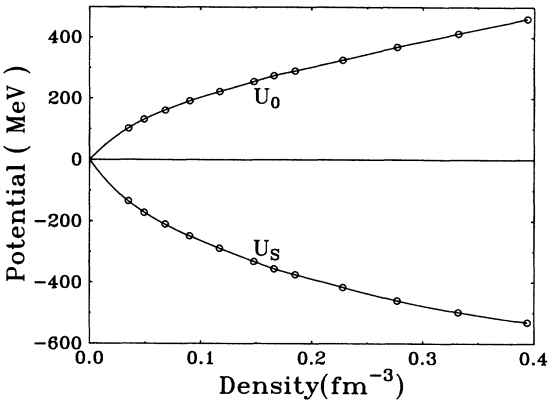


FIG. 1. Scalar and vector potentials $U_s$ and $U_0$ as functions of the density in nuclear matter. The circles are the DBHF results using Bonn $A$ potential [1]. The curves are obtained in terms of interpolations and extrapolations.

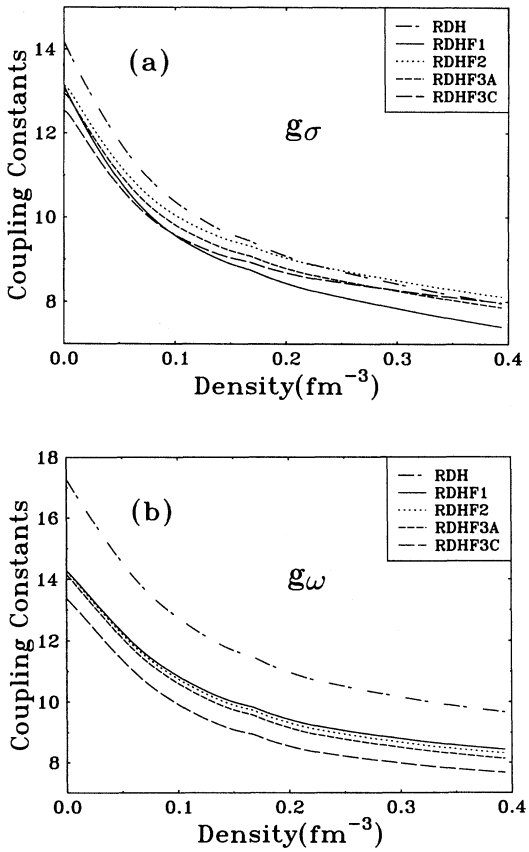


FIG. 2. Density-dependent coupling constants of $\sigma$ and $\omega$, $g_\sigma$ (a) and $g_\omega$ (b). They are deduced by reproducing the scalar and vector potentials of the DBHF results at each density from RMF and RHF analyses. The solid, dotted, dashed, and long-dashed curves correspond to the cases of $\sigma+\omega$ (RDHF1), $\sigma+\omega+\pi$ (RDHF2), and $\sigma+\omega+\pi+\rho$ (RDHF3A, RDHF3C), respectively. The dash-dotted curve is for the RDH.

meson are chosen to be the same as in the DBHF calculation, where $M = 938.9$ MeV, $m_\sigma = 550$ MeV, and $m_\omega = 782.6$ MeV. The pseudovector coupling for $\pi NN$, vector, and tensor coupling for $\rho NN$ is adopted. The masses and coupling constants of isovector mesons are fixed to be $m_\pi = 138$ MeV, $m_\rho = 770$ MeV, $\frac{f_\pi^2}{4\pi} = 0.08$, $\frac{g_\rho^2}{4\pi} = 0.55$, and $\frac{f_\rho}{g_\rho} = 3.7$ [5]. The density dependence of the coupling constants in various cases is shown in Fig. 2. The presence of the pion introduces a large repulsive force, so the scalar coupling constant becomes larger and the vector coupling constant gets smaller to balance the repulsive force, especially at normal and high densities. However, the pion contribution is partly canceled by the presence of $\rho$ mesons in symmetric nuclear matter. The tensor coupling of $\rho$ mesons has a large effect at high density. As a result, the coupling constant of $\sigma$ mesons becomes larger than that of $\omega$ mesons at high densities. It might be observed that the results obtained in this paper are somewhat different from those in Ref. [19]. The reason for this discrepancy is that the zero-range components of the pion exchange were removed there. The cases with and without the contact interactions have been discussed in more detail in Ref. [6]. It is found in our calculations that the effects of the contact interactions mainly cause a renormalization in $g_\sigma$ and $g_\omega$ coupling constants. The removal of the zero-range components of the pion and $\rho$ exchange would increase the binding energy and reduce the charge rms radius. No qualitative improvement has been found. Therefore only the cases with the zero-range components of the $\pi$ and $\rho$ exchange are presented in this paper.

### B. The ground state properties of finite nuclei

The ground state properties of five stable doubly closed-shell nuclei $^{16}$O, $^{40}$Ca, $^{48}$Ca, $^{90}$Zr, and $^{208}$Pb are calculated in the RDH and RDHF approaches with these density-dependent coupling constants. The set of coupled differential equations (17) is solved in the coordinate space following the method of Ref. [5]. Self-consistence is achieved by an iterative procedure. It is different from the matrix diagonalization method adopted in Refs. [16,17], where a truncation of a complete set of bases has been performed for both baryon and meson wave functions. Our computer code has been carefully checked with the results of Refs. [5,28].

In order to investigate the effect of the density dependence, the results for $^{16}$O and $^{40}$Ca obtained in the RMF and RHF with $\sigma + \omega$ (RHF1), $\sigma + \omega + \pi$ (RHF2), and $\sigma + \omega + \pi + \rho$ (RHF3) are listed in Table I. The coupling constants are determined to reproduce the DBHF results in nuclear matter (OBE potential $A$) at the saturation density $k_F = 1.40$ fm$^{-1}$. It should be mentioned that the results are different from those of the usual RMF and RHF calculations, where the coupling constants and scalar meson mass are adjusted to reproduce the empirical saturation properties of nuclear matter as well as the rms charge radius of $^{40}$Ca. Because of a relatively large saturation density obtained in the DBHF and the scalar meson mass $m_\sigma = 550$ MeV adopted in this calculation, the binding energies and rms charge radii calculated here are both much smaller than the experimental data. However, the main purpose of Table I is to show the difference in various cases mentioned above and compare with Table II to illustrate the effect of the density dependence. The saturation curves of nuclear matter calculated in the cases of the RMF (dotted curve), RHF1 (dashed one), RHF2 (dash-dotted one), and RHF3 (solid one) are plotted in Fig. 3 and compared with the DBHF results (circles). The finite nuclei calculations are mostly affected by the behavior of the self-energies at normal and low densities. Due to the hard behavior of the equation of state in those density-independent models, too small binding energies are observed at low densities. Therefore too weak potentials at the surface of finite nuclei are produced in those models. Calculations with density-dependent effective interactions are performed, where the coupling constants at each baryon density come from the

TABLE I. Ground state properties of $^{16}$O and $^{40}$Ca calculated in the RMF and RHF. The binding energy per nucleon $E_B/A$, the charge rms radius $r_{ch}$, and single-particle energies of proton states.

| | RMF | RHF1 | RHF2 | RHF3 |
|---|---|---|---|---|
| $^{16}$O | | | | |
| $E_B/A$ (MeV) | −5.62 | −6.02 | −4.86 | −5.67 |
| $r_{ch}$ (fm) | 2.48 | 2.39 | 2.53 | 2.57 |
| $1s_{1/2}$ (MeV) | 44.34 | 45.08 | 40.78 | 43.21 |
| $1p_{3/2}$ (MeV) | 18.96 | 21.15 | 17.50 | 18.51 |
| $1p_{1/2}$ (MeV) | 9.62 | 7.85 | 9.49 | 10.98 |
| $^{40}$Ca | | | | |
| $E_B/A$ (MeV) | −6.36 | −6.69 | −5.84 | −6.38 |
| $r_{ch}$ (fm) | 3.14 | 3.04 | 3.16 | 3.22 |
| $1d_{5/2}$ (MeV) | 16.54 | 18.61 | 15.72 | 16.35 |
| $2s_{1/2}$ (MeV) | 7.07 | 5.60 | 7.98 | 8.81 |
| $1d_{3/2}$ (MeV) | 6.92 | 5.70 | 6.50 | 7.79 |

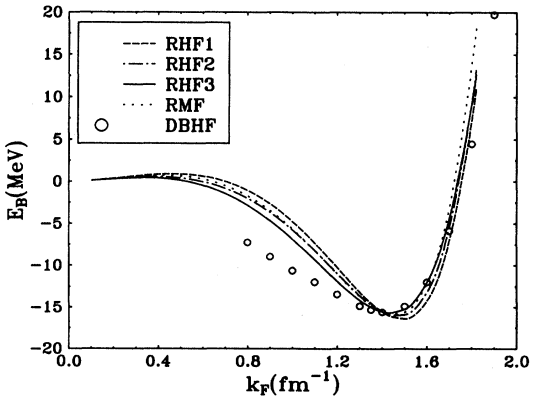


FIG. 3. Binding energy of nuclear matter as a function of the density. The curves are calculated in the relativistic density-independent models RMF (dotted curve), RHF1 (dashed curve), RHF2 (dash-dotted curve), and RHF3 (solid curve). The circles are the DBHF results.

TABLE II. Ground state properties of $^{16}$O, $^{40}$Ca, and $^{48}$Ca calculated in the RDH and RDHF. The binding energy per nucleon $E_B/A$, the charge rms radius $r_{ch}$, and single-particle energies of proton states.

| | RDH | RDHF1 | RDHF2 | RDHF3A | RDHF3B | RDHF3C | Expt. |
|---|---|---|---|---|---|---|---|
| $^{16}$O | | | | | | | |
| $E_B/A$ (MeV) | −7.44 | −7.48 | −6.96 | −7.29 | −7.57 | −7.41 | −7.98 |
| $r_{ch}$ (fm) | 2.59 | 2.50 | 2.64 | 2.61 | 2.59 | 2.68 | 2.73 |
| $1s_{1/2}$ (MeV) | 43.97 | 43.87 | 41.11 | 42.76 | 44.13 | 42.98 | $40 \pm 8$ |
| $1p_{3/2}$ (MeV) | 21.77 | 23.60 | 21.11 | 21.85 | 22.47 | 21.31 | 18.4 |
| $1p_{1/2}$ (MeV) | 16.16 | 16.08 | 15.60 | 16.07 | 16.47 | 15.72 | 12.1 |
| $^{40}$Ca | | | | | | | |
| $E_B/A$ (MeV) | −7.88 | −7.91 | −7.49 | −7.74 | −7.94 | −7.81 | −8.55 |
| $r_{ch}$ (fm) | 3.26 | 3.17 | 3.29 | 3.27 | 3.26 | 3.35 | 3.48 |
| $1d_{5/2}$ (MeV) | 19.27 | 21.17 | 19.08 | 19.52 | 19.89 | 18.95 | 15.5 |
| $2s_{1/2}$ (MeV) | 13.69 | 14.08 | 14.20 | 14.19 | 14.14 | 13.78 | 10.9 |
| $1d_{3/2}$ (MeV) | 13.29 | 13.48 | 12.77 | 13.09 | 13.35 | 12.67 | 8.3 |
| $^{40}$Ca | | | | | | | |
| $E_B/A$ (MeV) | −8.02 | −7.96 | −7.45 | −7.59 | −7.70 | −7.60 | −8.67 |
| $r_{ch}$ (fm) | 3.27 | 3.17 | 3.30 | 3.28 | 3.27 | 3.37 | 3.47 |
| $1d_{5/2}$ (MeV) | 24.35 | 29.17 | 24.34 | 26.37 | 27.96 | 26.72 | 20.0 |
| $2s_{1/2}$ (MeV) | 17.25 | 19.77 | 19.79 | 20.90 | 21.77 | 20.61 | 15.8 |
| $1d_{3/2}$ (MeV) | 18.68 | 21.79 | 23.05 | 24.92 | 26.38 | 23.53 | 15.3 |

parametrization of the DBHF result in nuclear matter as discussed in Sec. III A. Various cases, RDH, RDHF with $\sigma+\omega$ (RDHF1), $\sigma+\omega+\pi$ (RDHF2), and $\sigma+\omega+\pi+\rho$ (RDHF3), are investigated and the results for the nuclei $^{16}$O, $^{40}$Ca, $^{48}$Ca, $^{90}$Zr, and $^{208}$Pb are displayed in Tables II and III. In order to investigate the sensitivity of the $\rho$ meson coupling constant, two values of $\rho$ coupling constants are adopted in the calculations: $\frac{g_\rho^2}{4\pi}$ = 0.55 (RDHF3A) and 0.99 (RDHF3B) without tensor coupling. The results with $\rho NN$ tensor coupling ($\frac{g_\rho^2}{4\pi}$ = 0.55, $\frac{f_\rho}{g_\rho}$ = 3.7) are given as RDHF3C.

The importance of the density-dependent approaches is clearly demonstrated in Tables I and II. The calculations in either RMF or RHF with constant coupling constants produce much smaller binding energies of nucleons and rms radii in comparison with the experiments. In contrast, the approaches with density-dependent interactions increase both binding energy and charge radius, which implies removal from the so-called Coester band [8]. The results in the relativistic density-dependent approaches are greatly improved and close to the experimental values. The Fock exchange term in the $\sigma$-$\omega$ model reduces the charge radii, but has less influence on the binding energies. A large repulsion of the pion contribution at the interior of the nucleus is found. As a result, the energy levels of deeper states become shallow in the presence of the pion. Therefore the total binding energy is reduced and the charge radius is expanded. This effect is partly canceled by the $\rho$ meson exchange contribution. In a comparison of the RDHF3A with RDHF3B, the results are not sensitive to the strength of the $\rho$ meson coupling. The binding energies for the strong coupling constant of the $\rho$ meson $\frac{g_\rho^2}{4\pi}$ = 0.99 are about 2% bigger than those for $\frac{g_\rho^2}{4\pi}$ = 0.55 and the rms radii are reduced by less than 1%. However, the $\rho$ tensor coupling term has a relatively large effect. It can be found that the re-

TABLE III. Same as Table II, except for $^{90}$Zr and $^{208}$Pb.

| | RDH | RDHF1 | RDHF2 | RDHF3A | RDHF3B | RDHF3C | Expt. |
|---|---|---|---|---|---|---|---|
| $^{90}$Zr | | | | | | | |
| $E_B/A$ (MeV) | −7.94 | −7.92 | −7.55 | −7.67 | −7.78 | −7.68 | −8.71 |
| $r_{ch}$ (fm) | 4.00 | 3.89 | 4.02 | 4.00 | 3.99 | 4.10 | 4.27 |
| $2p_{3/2}$ (MeV) | 11.01 | 13.09 | 12.86 | 13.61 | 14.19 | 13.52 | 11.0 |
| $1f_{5/2}$ (MeV) | 13.14 | 15.61 | 16.67 | 18.12 | 19.24 | 16.93 | 12.3 |
| $2p_{1/2}$ (MeV) | 9.42 | 11.16 | 11.77 | 12.49 | 13.05 | 11.91 | 9.5 |
| $^{208}$Pb | | | | | | | |
| $E_B/A$ (MeV) | −7.38 | −7.09 | −6.75 | −6.70 | −6.61 | −6.69 | −7.87 |
| $r_{ch}$ (fm) | 5.17 | 5.02 | 5.18 | 5.17 | 5.17 | 5.30 | 5.50 |
| $2d_{5/2}$ (MeV) | 9.94 | 14.40 | 13.63 | 15.73 | 17.32 | 15.68 | 9.7 |
| $2d_{3/2}$ (MeV) | 8.23 | 12.44 | 13.01 | 15.09 | 16.64 | 13.54 | 8.4 |
| $3s_{1/2}$ (MeV) | 7.06 | 11.36 | 11.30 | 13.26 | 14.78 | 12.72 | 8.0 |
| $1h_{11/2}$ (MeV) | 8.09 | 13.82 | 8.97 | 11.28 | 13.03 | 11.43 | 9.4 |

sults of both binding energy and rms charge radius in the RDHF3C are improved. The binding energies of nuclei are increased slightly, but the charge radii of nuclei are improved greatly in comparison with experiments.

Figure 4 shows the density distribution of nuclei. The dense dotted curves are the results of the RHF3, corresponding to the case in the fourth column of Table I. The dashed, dash-dotted, dotted, and solid curves correspond to those of the RDH and RDHF (RDHF1, RDHF3A, RDHF3C) without and with isovector mesons, respectively. It is found that the charge densities are reduced at the nuclear interior and have a long tail due to the relatively strong coupling constants at the nuclear surface in the density-dependent calculations. The Fock contributions of $\sigma$ and $\omega$ in the RDHF produce a squeezing effect and give a large central density. The repulsive contribution of $\pi$ reduces the interior density and the results of the RDHF3A are very close to those of the RDH. Though the densities at the center are still higher than the experimental data, which implies small rms radii, it is a parameter-free calculation in the sense that no parameters are adjusted for the calculations of the many-body problem. However, the results with density-dependent coupling constants are in reasonably good agreement with the experiments.

As is well known, nonrelativistic BHF calculations with various two-body nucleon-nucleon potentials, such as Reid soft-core and Hamada-Johnston potentials, reveal a "Coester" band in the dependence of $1/r_c$ on $E_B/A$. In the RMF or RHF calculations, the dependence of $1/r_c$ on $E_B/A$, with variation of the scalar meson mass, and therefore the variation of the coupling constants, formed a new "Coester" band. A better estimate of the merits of the present work can be expected upon comparison with the BHF "Coester" band and RHF "Coester" band. Those "Coester" bands are plotted in Fig. 5 for $^{16}$O and $^{40}$Ca; the dash-dotted line indicates the BHF "Coester" band, which is taken from so-called generalized BHF calculations by Kümmel *et al.* [9]. The dotted and dashed lines represent the RHF results, which are obtained in the RHF3 by varying the scalar meson mass as well as the coupling constants to reproduce the nuclear matter saturation properties at $k_F = 1.40$ fm$^{-1}$ (1) and $k_F = 1.30$ fm$^{-1}$ (2) resulting from the DBHF approach. The results in the case of the RDHF3C are displayed by a solid line in the figure. The density-dependent approach forms a new line away from the "Coester" band of the conventional BHF and seems to be much closer to the experimental values than the BHF and RHF calculations.

The spin-orbit splittings of nuclei are given in Table IV. It can be seen that the spin-orbit splitting in the RMF and RHF approaches is larger than the experimen-

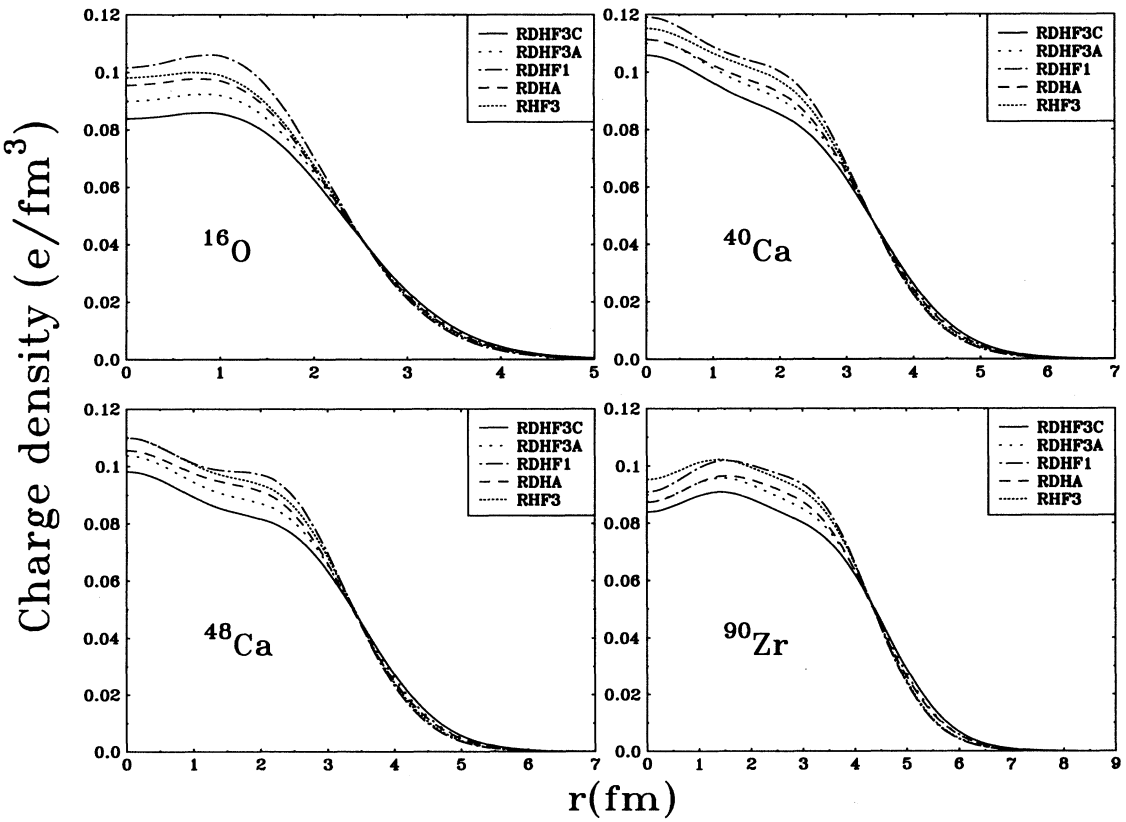


FIG. 4. Charge density distribution of various nuclei. The curves are the results of RDH (dashed), RDHF with $\sigma + \omega$ only (dash-dotted), RDHF with $\sigma + \omega + \pi + \rho$ (solid for 3C and dotted for 3A), and RHF with $\sigma + \omega + \pi + \rho$ (dense-dotted).

TABLE IV. Spin-orbit splittings of protons for the $1p$ shell in $^{16}$O and the $1d$ shell in $^{40}$Ca and $^{48}$Ca.

| Nuclei | RMF | RHF1 | RHF3 | RDH | RDHF1 | RDHF3A | RDHF3C | Expt. |
|---|---|---|---|---|---|---|---|---|
| $^{16}$O | 9.34 | 13.30 | 7.53 | 5.61 | 7.52 | 5.78 | 5.60 | 6.3 |
| $^{40}$Ca | 9.62 | 12.82 | 8.56 | 5.78 | 7.69 | 6.43 | 6.28 | 7.2 |
| $^{48}$Ca | 9.32 | 12.52 | 5.32 | 5.67 | 7.37 | 1.45 | 3.19 | 4.3 |

tal data, which indicates the larger spin-orbit force. It is known that the spin-orbit force is related to the derivative of the potentials with respect to the space and is a surface effect. The density-dependent approaches reduce the sharp surface and, therefore, reduce the spin-orbit splitting. The Fock terms of the $\sigma$ and $\omega$ exchange increase the spin-orbit splitting, while the $\pi$ and $\rho$ exchanges give the opposite contribution. A large reduction of the spin-orbit splitting due to pion-exchange is found, especially for heavy nuclei with a large neutron excess. A flip of the spin-orbit splitting of neutron states in $^{208}$Pb is observed in the calculation of RDHF with all mesons included, which is certainly not physical. It might indicate that the free coupling constants of the isovector mesons adopted in the RDHF are too strong for the nuclear structure calculation. A similar observation was obtained in the calculation of the relativistic optical potential in the RHF approach [26]. The density-dependent coupling constants for isovector mesons may also be required.

It is known that the single-particle densities are not directly provided by experiments. The only way to gain some insights in the single-particle distribution is to study the difference between density distributions of nearby nuclei. In Fig. 6(a), we give the charge distribution difference between $^{40}$Ca and $^{48}$Ca, multiplied by $r^2$. The difference of the neutron densities between $^{40}$Ca and $^{48}$Ca are plotted in Fig. 6(b). The shaded area presents the experimental data, the dashed curve is the results of the RDH, the dotted one the results of RDHF1, and the solid one is obtained in the case of RDHF3C. It can be

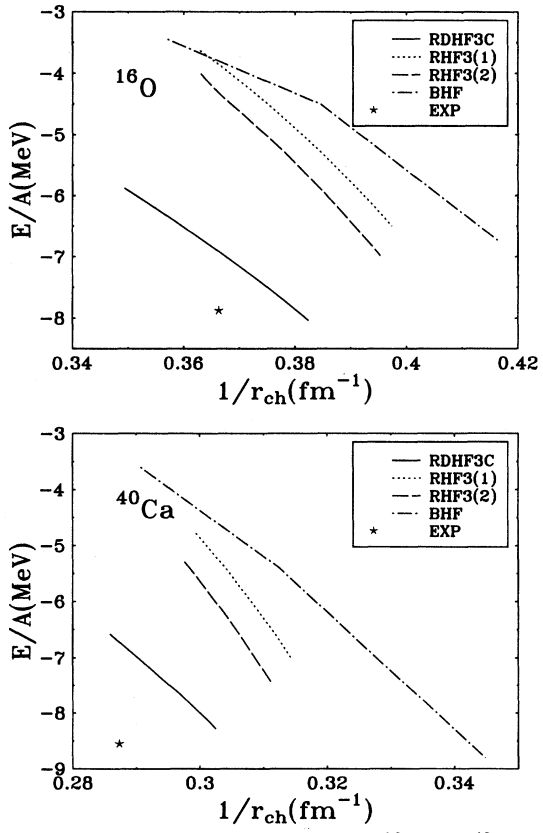


FIG. 5. Binding energy versus $1/r_{ch}$ for $^{16}$O and $^{40}$Ca. The dash-dotted line is taken from the work of Kümmel *et al.* [9]. The dotted and dashed lines are obtained in the RHF3 with changing $\sigma$ meson mass for $k_F = 1.4$ fm$^{-1}$ (1) and $k_F = 1.3$ fm$^{-1}$ (2), respectively. The solid lines are the results of RDHF3C. The experimental data are displayed by a star.

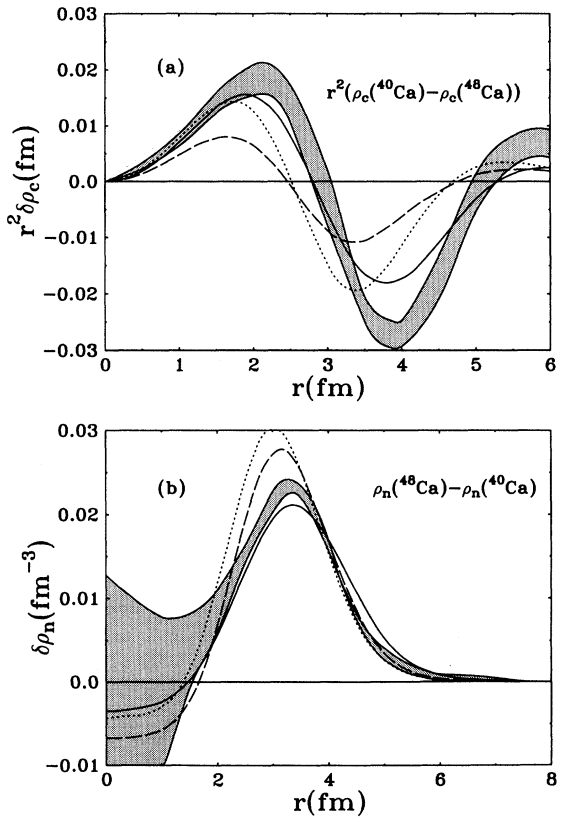


FIG. 6. Differences between charge densities (a) and neutron density (b) of $^{40}$Ca and $^{48}$Ca. The dashed curve corresponds to the RDH and the dotted curve to the RDHF1. The solid line corresponds to the RDHF3C. The shaded area indicates the experimental data.

TABLE V. Neutron skin thickness $\Delta_{np} = r_n - r_p$ for $^{16}$O, $^{40}$Ca, $^{48}$Ca, $^{90}$Zr, and $^{208}$Pb. The DBHF results are taken from [20].

| Nuclei | RHF3 | DBHF | RDHF1 | RDHF3C | Expt. |
|---|---|---|---|---|---|
| $^{16}$O | −0.03 | −0.03 | −0.03 | −0.02 | −0.02 |
| $^{40}$Ca | −0.05 | −0.06 | −0.05 | −0.04 | −0.07–0.10 |
| $^{48}$Ca | 0.23 | 0.13 | 0.15 | 0.22 | 0.16–0.23 |
| $^{90}$Zr | 0.11 | 0.04 | 0.07 | 0.11 | 0.07 |
| $^{208}$Pb | 0.27 | 0.08 | 0.17 | 0.22 | 0.04–0.16 |

seen that the results obtained in the RDHF3C are superior to those of the RDH and RDHF1 in comparison with experiments. This implies that the isospin dependence cannot be correctly described by the RDH as well as RDHF1 without including isovector mesons.

Neutron skin thicknesses is an important quantity to study isotope shifts. It is defined as the difference between neutron and proton rms radii: $\Delta_{np} = r_n - r_p$. The neutron skin thicknesses of $^{16}$O, $^{40}$Ca, $^{48}$Ca, $^{90}$Zr and $^{208}$Pb are given in Table V, and the $\Delta_{np}$ versus the asymmetry parameter $(N-Z)/A$ for those nuclei is shown in Fig. 7. The results of the RDHF3C seem to be similar to those of the RMF at small asymmetry parameters. But it goes down as the asymmetry parameter increases in the region of lead, which has similar behavior to that obtained in Ref. [20]. More information of the isospin dependence of the ground state properties is required.

## IV. CONCLUSION

In summary, the RDH and RDHF approaches with the density-dependent effective coupling constants of isoscalar mesons can incorporate the DBHF results and contain the nucleon-nucleon correlation effects. Inclusion of the $NN$ correlation causes a substantial improvement in the microscopic description of bulk properties of nuclei. The Fock exchange terms are not negligible, though the exchange contributions are relatively weaker than those of the Hartree direct term in the relativistic approach and their contribution to the binding energy may be partly compensated by the variation of the coupling constants. The important contributions from the isovector $\pi$ meson and, to some extent, the $\rho$ meson are not included in the mean field approach. It is found that the isovector $\pi$ and $\rho$ mesons play an important role in the spin-orbit splitting as well as the isospin-dependent quantities. The tensor coupling of the $\rho$ meson gives a constructive contribution to the binding energy, especially the rms charge radius, and therefore improves the agreement with the experimental data. More information of the isospin dependence of nuclear properties is required to provide constraints on the coupling constants of isovector $\pi$ and $\rho$ mesons in the nuclear medium.

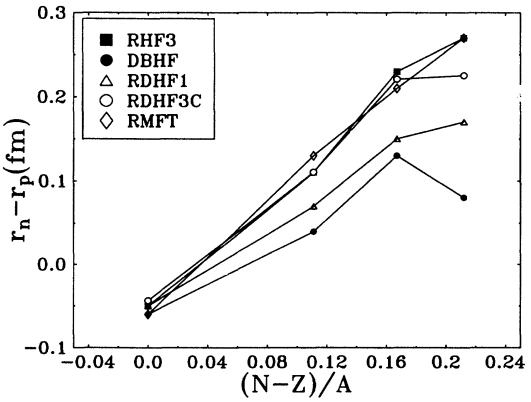


FIG. 7. $\Delta_{np}$ versus the asymmetry parameter for various cases and the results of the DBHF approach are taken from Ref. [20].

## ACKNOWLEDGMENTS

One of the authors (Z.M.) would like to thank J.-F. Mathiot for useful discussions. This work was supported by The National Natural Science Foundation of China.

## APPENDIX A: SELF-ENERGY IN NUCLEAR MATTER

In the Hartree-Fock approach, the nucleon self-energy in nuclear matter coming from the exchange of the isovector pseudoscalar meson $\pi$ can be written as follows:

$$\Sigma_s^\pi(k) = \frac{3}{8\pi^2 k}\int_0^{k_F} dq\, q \left(\frac{f_\pi}{m_\pi}\right)^2 \hat{M}\left(2kq - \frac{1}{2}m_\pi^2\Theta_\pi\right), \tag{A1}$$

$$\Sigma_0^\pi(k) = -\frac{3}{8\pi^2 k}\int_0^{k_F} dq\, q \left(\frac{f_\pi}{m_\pi}\right)^2 \left[-\frac{1}{2}m_\pi^2\Theta_\pi + 2kq\right], \tag{A2}$$

$$\Sigma_v^\pi(k) = -\frac{3}{8\pi^2 k^2}\int_0^{k_F} dq\, q \left(\frac{f_\pi}{m_\pi}\right)^2 \times \left[q\hat{Q}k\Theta_\pi - \hat{Q}(k^2+q^2)\Phi_\pi\right]. \tag{A3}$$

The contribution to the self-energy of a nucleon from isovector vector meson $\rho$ can be written as

$$\Sigma_s^\rho(k) = \frac{3}{8\pi^2 k}\int_0^{k_F} dq\, q\Bigg\{-2g_\rho^2\hat{M}\Theta_\rho + 3\left(\frac{f_\rho}{2M}\right)^2 \hat{M}\left(2kq - \frac{1}{2}m_\rho^2\Theta_\rho\right) + 3g_\rho\left(\frac{f_\rho}{2M}\right)\left[q\hat{Q}\Theta_\rho - 2k\hat{Q}\Phi_\rho\right]\Bigg\}, \tag{A4}$$

$$\Sigma_0^\rho(k) = -\frac{3}{8\pi^2 k}\int_0^{k_F} dq\, q\Bigg\{g_\rho^2\Theta_\rho + \left(\frac{f_\rho}{2M}\right)^2\left[2kq - \frac{1}{2}m_\rho^2\Theta_\rho\right]\Bigg\}, \tag{A5}$$

$$\Sigma_v^\rho(k) = -\frac{3}{8\pi^2 k^2}\int_0^{k_F} dq\; q\Big\{2g_\rho^2\hat{Q}\Phi_\rho$$

$$+2\left(\frac{f_\rho}{2M}\right)^2\left[kq\hat{Q}\Theta_\rho - \hat{Q}(k^2+q^2-\frac{1}{2}m_\rho^2)\Phi_\rho\right]$$

$$-3g_\rho\left(\frac{f_\rho}{2M}\right)(k\hat{M}\Theta_\rho - 2q\hat{M}\Phi_\rho)\Big\}. \qquad \text{(A6)}$$

## APPENDIX B: FOCK TERM EXPRESSIONS

The quantities $X$ and $Y$ in Eq. (17) can be written as the sum of contributions coming from various mesons. In the following, we often need the reduced matrix elements of the tensorial operators $Y_L^m(\hat{r})$ and

$$T_{JL}^M \equiv \sum_{mk}\langle L1mk|JM\rangle Y_L^m(\hat{r})\sigma^k.$$

They are given as follows:

$$\langle a||Y_L||b\rangle = \begin{cases} (4\pi)^{-\frac{1}{2}}\hat{j}_a\hat{j}_b\hat{L}(-1)^{j_b-L-\frac{1}{2}}\begin{pmatrix} j_a & j_b & L \\ \frac{1}{2} & -\frac{1}{2} & 0\end{pmatrix} & \text{if } l_a+l_b+L \text{ is even} \\ 0 & \text{if } l_a+l_b+L \text{ is odd,}\end{cases} \qquad \text{(B1)}$$

$$\langle a||T_{JL}||b\rangle = \left(\frac{6}{4\pi}\right)^{\frac{1}{2}}(-1)^{l_a}\hat{j}_a\hat{j}_b\hat{l}_a\hat{l}_b\hat{J}\hat{L}\begin{pmatrix} l_a & L & l_b \\ 0 & 0 & 0\end{pmatrix}\begin{Bmatrix} j_a & j_b & J \\ l_a & l_b & L \\ \frac{1}{2} & \frac{1}{2} & 1\end{Bmatrix},$$

where $\hat{J} = \sqrt{2J+1}$.

The exchange term from the scalar $\sigma$ meson is determined to be

$$\begin{pmatrix} -X^\sigma(r) \\ Y^\sigma(r)\end{pmatrix} = g_\sigma[\rho_B(r)]m_\sigma\hat{j}_a^{-2}\sum_b \delta_{q_aq_b}\begin{pmatrix} F_b(r) \\ G_b(r)\end{pmatrix}\sum_L\left|\langle a||Y_L||b\rangle\right|^2$$
$$\times\int_0^\infty g_\sigma[\rho_B(r')][G_aG_b - F_aF_b]_{r'}\tilde{I}_L(m_\sigma r_<)\tilde{K}_L(m_\sigma r_>)dr', \qquad \text{(B2)}$$

where the sum over $b$ runs over all occupied states.

The expressions for the vector $\omega$ meson are split into timelike and spacelike parts, with respect to the $\gamma_0$ and $\gamma$ couplings. The time component is

$$\begin{pmatrix} -X_0^\omega(r) \\ Y_0^\omega(r)\end{pmatrix} = g_\omega[\rho_B(r)]m_\omega\hat{j}_a^{-2}\sum_b \delta_{q_aq_b}\begin{pmatrix} F_b(r) \\ -G_b(r)\end{pmatrix}\sum_L\left|\langle a||Y_L||b\rangle\right|^2$$
$$\times\int_0^\infty g_\omega[\rho_B(r')][G_aG_b + F_aF_b]_{r'}\tilde{I}_L(m_\omega r_<)\tilde{K}_L(m_\omega r_>)dr'. \qquad \text{(B3)}$$

The space component is

$$\begin{pmatrix} -X^\omega(r) \\ Y^\omega(r)\end{pmatrix} = -\frac{g_\omega[\rho_B(r)]}{4\pi}m_\omega\sum_{b,L}\frac{1}{2}[1+(-1)^{l'_a+l_b+L}]\delta_{q_aq_b}\hat{j}_b^2\hat{L}^2\begin{pmatrix} G_b(r) \\ -F_b(r)\end{pmatrix}$$
$$\times\int_0^\infty g_\omega[\rho_B(r')]\Bigg\{\begin{pmatrix} G_aF_b \\ F_aG_b\end{pmatrix}\begin{pmatrix} j_a & j_b & L \\ \frac{1}{2} & -\frac{1}{2} & 0\end{pmatrix}^2$$
$$+\begin{pmatrix} F_aG_b \\ G_aF_b\end{pmatrix}\left[2\begin{pmatrix} J(l'_a,L,l_b) \\ J(l_a,L,l'_b)\end{pmatrix} - \begin{pmatrix} j_a & j_b & L \\ \frac{1}{2} & -\frac{1}{2} & 0\end{pmatrix}^2\right]\Bigg\}\tilde{I}_L(m_\omega r_<)\tilde{K}_L(m_\omega r_>)dr', \qquad \text{(B4)}$$

where $a' = (q_a, n_a, l'_a, j_a)$ with $l'_a = 2j_a - l_a$, and

$$J(l'_a, L, l_b) = \begin{pmatrix} l'_a & L & l_b \\ 0 & 0 & 0\end{pmatrix}^2.$$

The contribution from the isovector pseudoscalar $\pi$ meson with a peudovector coupling is as follows

$$\begin{pmatrix} -X^{\pi}(r) \\ Y^{\pi}(r) \end{pmatrix} = f_{\pi}^2 \hat{j}_a^{-2} \sum_b (2-\delta_{q_a q_b}) \Bigg\{ \frac{j_a^2 j_b^2}{8\pi} \frac{(G_a G_b + F_a F_b)_r}{m_{\pi}^2 r^2} \begin{pmatrix} -F_b(r) \\ G_b(r) \end{pmatrix} - m_{\pi} \sum_L \hat{L}^{-4} \left| \langle a||Y_L||b' \rangle \right|^2 \sum_{L_1,L_2} \begin{pmatrix} F_b(r)[\kappa_{ab} - \alpha(L_1)] \\ G_b(r)[\kappa_{ab} + \alpha(L_1)] \end{pmatrix} i^{L_2 - l_1} \times \int_0^{\infty} [\{\kappa_{ab} + \alpha(L_2)\} G_a G_b - \{\kappa_{ab} - \alpha(L_2)\} F_a F_b]_{r'} R_{L_1,L_2}(m_{\pi} r, m_{\pi} r') dr' \Bigg\}, \tag{B5}$$

where the notations

$$\kappa_{ab} = \kappa_a + \kappa_b$$

$$\alpha(L_1) = \begin{cases} -L & \text{if } L_1 = L-1, \\ L+1 & \text{if } L_1 = L+1, \end{cases}$$

$$R_{L_1 L_2}(mr, mr') = \tilde{I}_{L_1}(mr) \tilde{K}_{L_2}(mr') \theta(r'-r) + \tilde{K}_{L_1}(mr) \tilde{I}_{L_2}(mr') \theta(r-r')$$

are introduced. The $L_1$ and $L_2$ can only take two values $L+1$ or $L-1$.

The vector part of the $\rho NN$ coupling in our Lagrangian gives $X(r)$ and $Y(r)$ which are formally identical to those of the $\omega$ meson, expect for the isospin factor $\delta_{q_a q_b}$ replaced by $2 - \delta_{q_a q_b}$ and $m_{\omega}$, and $g_{\omega}[\rho_B(r)]$ replaced by $m_{\rho}$ and $g_{\rho}$ . The tensor term gives rise to two types of contributions. They are proportional to $f_{\rho}^2$ and $f_{\rho} g_{\rho}$, and are denoted, respectively, by $(X^{(T)}, Y^{(T)})$ and $(X^{(VT)}, Y^{(VT)})$. Similarly, they can be split into timelike and spacelike components. The time component of $X^{(T)}$ and $Y^{(T)}$ is written as

$$\begin{pmatrix} -X_0^{(T)}(r) \\ Y_0^{(T)}(r) \end{pmatrix} = -\left(\frac{f_{\rho}}{2M}\right)^2 m_{\rho}^2 \hat{j}_a^{-2} \sum_b (2-\delta_{q_a q_b}) \Bigg\{ \frac{\hat{j}_a^2 \hat{j}_b^2}{8\pi} \frac{(G_a F_b + F_a G_b)_r}{m_{\rho}^2 r^2} \begin{pmatrix} -G_b(r) \\ F_b(r) \end{pmatrix} - m_{\rho} \sum_L \hat{L}^{-4} \left| \langle a||Y_L||b \rangle \right|^2 \sum_{L_1,L_2} \begin{pmatrix} G_b(r)[\tilde{\kappa}_{ab} - \alpha(L_1)] \\ F_b(r)[\tilde{\kappa}_{ab} + \alpha(L_1)] \end{pmatrix} i^{L_2 - L_1} \times \int_0^{\infty} [\{\tilde{\kappa}_{ab} + \alpha(L_2)\} G_a F_b - \{\tilde{\kappa}_{ab} - \alpha(L_2)\} F_a G_b]_{r'} R_{L_1,L_2}(m_{\rho} r, m_{\rho} r') dr' \Bigg\}, \tag{B6}$$

where $\tilde{\kappa}_{ab} = \kappa_a - \kappa_b$. The space component of $X^{(T)}$ and $Y^{(T)}$ is

$$\begin{pmatrix} -X^{(T)}(r) \\ Y^{(T)}(r) \end{pmatrix} = 6 \left(\frac{f_{\rho}}{2M}\right)^2 m_{\rho}^2 \hat{j}_a^{-2} \sum_b (2-\delta_{q_a q_b}) \begin{pmatrix} -F_b(r) \\ G_b(r) \end{pmatrix} \sum_{L J L_1 L_2} f_{LJ}(L_1) f_{LJ}(L_2) \times \begin{pmatrix} \langle a'||T_{JL_1}||b' \rangle \\ \langle a||T_{JL_1}||b \rangle \end{pmatrix} \int_0^{\infty} [\langle a||T_{JL_2}||b \rangle G_a G_b - \langle a'||T_{JL_2}||b' \rangle F_a F_b]_{r'} \times \left[ m_{\rho} R_{L_1 L_2}(m_{\rho} r, m_{\rho} r') - \frac{\delta(r-r')}{m_{\rho}^2 r'^2} \right] dr', \tag{B7}$$

where we have introduced

$$f_{LJ}(L_1) \equiv \hat{L} \hat{L}_1 \begin{pmatrix} L_1 & L & 1 \\ 0 & 0 & 0 \end{pmatrix} \begin{Bmatrix} L_1 & L & 1 \\ 1 & 1 & J \end{Bmatrix}.$$

The time component of the $VT$ contribution is

$$\begin{pmatrix} -X_0^{(VT)}(r) \\ Y_0^{(VT)}(r) \end{pmatrix} = \left(\frac{g_{\rho} f_{\rho}}{2M}\right) m_{\rho}^2 \hat{j}_a^{-2} \sum_b (2-\delta_{q_a q_b}) \sum_{L L_1} (-1)^{L_1} \hat{L}_1 \begin{pmatrix} L_1 & L & 1 \\ 0 & 0 & 0 \end{pmatrix} \Bigg\{ \begin{pmatrix} -G_b(r) \langle a'||T_{LL_1}||b \rangle \\ F_b(r) \langle a||T_{LL_1}||b' \rangle \end{pmatrix} \times \int_0^{\infty} [\langle a||Y_L||b \rangle G_a G_b + \langle a'||Y_L||b' \rangle F_a F_b]_{r'} S_{LL_1}(r, r') dr' + \begin{pmatrix} -F_b(r) \langle a'||Y_L||b' \rangle \\ G_b(r) \langle a||Y_L||b \rangle \end{pmatrix} \times \int_0^{\infty} [\langle a||T_{LL_1}||b' \rangle G_a F_b + \langle a'||T_{LL_1}||b \rangle F_a G_b]_{r'} S_{LL_1}(r', r) dr' \Bigg\}. \tag{B8}$$

The space component of the $VT$ contribution is

$$\begin{pmatrix} -X^{(VT)}(r) \\ Y^{(VT)}(r) \end{pmatrix} = -\sqrt{6}\left(\frac{g_\rho f_\rho}{2M}\right) m_\rho^2 \hat{j}_a^{-2} \sum_b (2-\delta_{q_a q_b}) \sum_{JLL_1} (-1)^J f_{LJ}(L_1)$$
$$\times \Bigg\{ \begin{pmatrix} F_b(r)\langle a'||T_{JL_1}||b'\rangle G_b(r)\langle a||T_{JL_1}||b\rangle \end{pmatrix} \int_0^\infty [\langle a||T_{JL}||b'\rangle G_a F_b - \langle a'||T_{JL}||b\rangle F_a G_b]_{r'} S_{LL_1}(r,r')dr'$$
$$\times \begin{pmatrix} G_b(r)\langle a'||T_{JL}||b\rangle \\ F_b(r)\langle a||T_{JL}||b'\rangle \end{pmatrix} \int_0^\infty [\langle a||T_{JL_1}||b\rangle G_a G_b - \langle a'||T_{JL_1}||b'\rangle F_a F_b]_{r'} S_{LL_1}(r,r')dr' \Bigg\}, \tag{B9}$$

where

$$S_{LL_1}(r,r') = \tilde{I}_{L_1}(m_\rho r)\tilde{K}_L(m_\rho r')\theta(m_\rho(r'-r)) - \tilde{I}_L(m_\rho r')\tilde{K}_{L_1}(m_\rho r)\theta(m_\rho(r-r')).$$


[1] B.D. Serot and J.D. Walecka, in *Advances in Nuclear Physics*, edited by J.W. Negele and E. Vogt (Plenum, New York, 1986), Vol. 16.

[2] Y.K. Gambhir, P. Ring, and A. Thimet, Ann. Phys. (N.Y.) **198**, 132 (1990).

[3] H. Toki, Y. Sugahara, D. Hirata, I. Tanihata, and B. Carlson, Nucl. Phys. **A524**, 633 (1991).

[4] M.M. Sharma, G.A. Lalazissis, W. Hillebrandt, and P. Ring, Phys. Rev. Lett. **72**, 1431 (1994).

[5] A. Bouyssy, J.-F. Mathiot, N. Van Giai, and S. Marcos, Phys. Rev. C **36**, 380 (1987).

[6] P. Bernardos *et al.*, Phys. Rev. C **48**, 2665 (1993).

[7] J.K. Zhang and D.S. Onley, Phys. Rev. C **43**, 942 (1991); **46**, 1677 (1992); **48**, 2697 (1993).

[8] F. Coester, S. Cohen, B.D. Day, and C.M. Vincent, Phys. Rev. C **1**, 769 (1970).

[9] H. Kümmel, K.H. Lührmann, and J.G. Zabolitzky, Phys. Rep. **36**, 1 (1978).

[10] M.R. Anastasio, L.S. Celenza, W.S. Pong, and C.M. Shakin, Phys. Rep. **100**, 327 (1983).

[11] B. ter Haar and R. Malfliet, Phys. Rep. **149**, 207 (1987).

[12] C.J. Horowitz and B.D. Serot, Nucl. Phys. **A464**, 613 (1987).

[13] R. Brockmann and R. Machleidt, Phys. Lett. **149B**, 283 (1984); Phys. Rev. C **42**, 1965 (1990).

[14] H. Müther, R. Machleidt, and R. Brockmann, Phys. Rev. C **42**, 1981 (1990).

[15] S. Gmuca, J. Phys. G **17**, 1115 (1991); Z. Phys. A **342**, 387 (1992).

[16] R. Brockmann and H. Toki, Phys. Rev. Lett. **68**, 3408 (1992).

[17] R. Fritz, H. Müther, and R. Machleidt, Phys. Rev. Lett. **71**, 46 (1993).

[18] Zhong-yu Ma, Hua-lin Shi, and Bao-qiu Chen, Chin. Phys. Lett. **12**, 295 (1995).

[19] R. Fritz and H. Müther, Phys. Rev. C **49**, 633 (1994).

[20] H.F. Boersma and R. Malfliet, Phys. Rev. C **49**, 233 (1994); **49**, 1495 (1994).

[21] Zhong-yu Ma, Hua-lin Shi, and Bao-qiu Chen, Phys. Rev. C **50**, 3170 (1994).

[22] R. Machleidt, in *Advances in Nuclear Physics*, edited by J.W. Negele and E. Vogt (Plenum, New York, 1989), Vol. 19, p. 189.

[23] C.J. Horowitz and B.D. Serot, Nucl. Phys. **A399**, 529 (1983).

[24] A.L. Fetter and J.D. Walecka, *Quantum Theory of Many-Particle Systems* (McGraw-Hill, New York, 1971).

[25] Zhong-yu Ma, Ping Zhu, Ying-qi Gu, and Yi-zhong Zhou, Nucl. Phys. **A490**, 619 (1989).

[26] G.Q. Li and R. Machleidt, Phys. Rev. C **48**, 2707 (1993).

[27] Zhong-yu Ma and Bao-qiu Chen, Commun. Theor. Phys. **21**, 59 (1994).

[28] R. Fritz (private communication).